Proliferation of Functional Hair Cells in Vivo in the Absence of the Retinoblastoma Protein

Cyrille Sage,[1] Mingqian Huang,[1] Kambiz Karimi,[2] Gabriel Gutierrez,[3] Melissa A. Vollrath,[4] Duan-Sun Zhang,[4] Jaime García-Añoveros,[5] Philip W. Hinds,[3] Jeffrey T. Corwin,[2] David P. Corey,[4] Zheng-Yi Chen[1]*

In mammals, hair cell loss causes irreversible hearing and balance impairment because hair cells are terminally differentiated and do not regenerate spontaneously. By profiling gene expression in developing mouse vestibular organs, we identified the retinoblastoma protein (pRb) as a candidate regulator of cell cycle exit in hair cells. Differentiated and functional mouse hair cells with a targeted deletion of *Rb1* undergo mitosis, divide, and cycle, yet continue to become highly differentiated and functional. Moreover, acute loss of *Rb1* in postnatal hair cells caused cell cycle reentry. Manipulation of the pRb pathway may ultimately lead to mammalian hair cell regeneration.

In fish, amphibians, and birds, regeneration of sensory hair cells through asymmetric cell divisions of supporting cells can contribute to recovery of hearing and balance after hair cell loss caused by trauma or toxicity (*1*, *2*). Mammalian hair cells do not spontaneously regenerate, even though supporting cells in vestibular sensory epithelia retain a limited ability to divide (*3*, *4*). Consequently, hair cell death in mammals often leads to permanent impairment of hearing and balance.

As the inner ear develops, hair cell progenitor cells exit from the cell cycle and, like neurons, terminally differentiate. Negative cell cycle regulators apparently maintain the postmitotic status of hair cells and contribute to their terminal differentiation. The cyclin-dependent kinase inhibitors p27Kip1 and p19Ink4d participate in cell cycle exit of hair cell progenitors and in hair cell apoptosis, respectively (*5*, *6*). However, the key regulators of cell cycle exit and concomitant hair cell terminal differentiation remain elusive.

The retinoblastoma protein pRb, encoded by the retinoblastoma gene *Rb1*, functions in cell cycle exit, differentiation, and survival (*7*, *8*). pRb is a member of the pocket protein family, which includes p107 (encoded by *Rbl1*) and p130 (encoded by *Rbl2*). Like pRb, p107 and p130 cause cell cycle arrest when overexpressed (*9*).

Germline pRb$^{-/-}$ animals die in utero around embryonic day (E) 13.5, with severe defects in lens development, hematopoiesis, myogenesis, osteogenesis, and neurogenesis (*7*, *10*–*12*). In both the central and peripheral nervous systems, neurons undergo ectopic mitoses and subsequent apoptosis (*11*, *13*). Mice with *Rb1* conditionally deleted in the central nervous system show an increase in neuronal number due to aberrant S phase entry, without apoptosis (*14*–*16*). However, it

[1]Neurology Service, MGH-HMS Center for Nervous System Repair, Massachusetts General Hospital and Harvard Medical School, Boston, MA 02114, USA. [2]Department of Neuroscience, University of Virginia School of Medicine, Charlottesville, VA 22908, USA. [3]Radiation Oncology, Molecular Oncology Research Institute, Tufts-New England Medical Center, Boston, MA 02111, USA. [4]Howard Hughes Medical Institute and Department of Neurobiology, Harvard Medical School, Boston, MA 02115, USA. [5]Departments of Anesthesiology, Physiology, and Neurology, Northwestern University Institute for Neuroscience, Chicago, IL 60611, USA.

*To whom correspondence should be addressed. E-mail: zhengyi@helix.mgh.harvard.edu

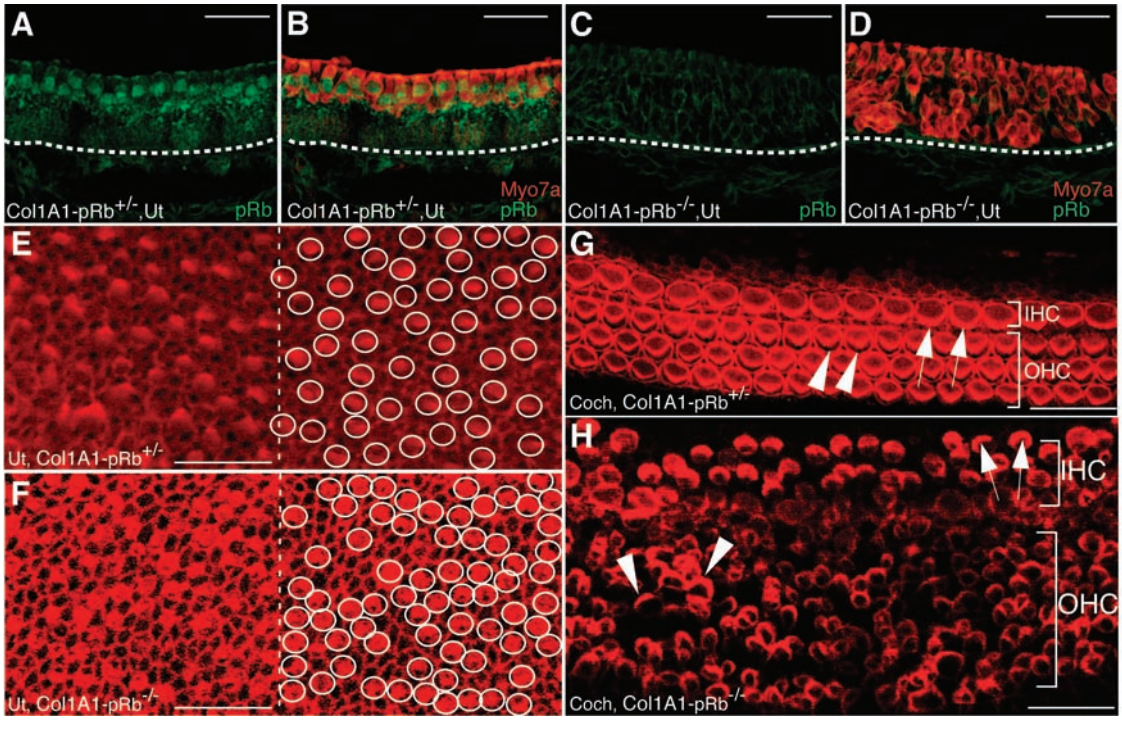

Fig. 1. Expression of *Rb1* in the inner ear and increased hair cell numbers in Col1A1-pRb$^{-/-}$ mice. (**A** and **B**) An antibody to pRb primarily stained hair cells in an E18.5 control utricle; an antibody to myosin-7a (Myo7a) marked hair cells. (**C** and **D**) pRb was absent in an E18.5 Col1A1-pRb$^{-/-}$ utricle; note multiple-layer hair cells in Col1A1-pRb$^{-/-}$ utricle. Dashed lines show basal lamina. (**E** to **H**) Confocal images of rhodamine phalloidin-labeled hair bundles in the E18.5 utricular macula [(E) and (F)] and midturn of the cochlea [(G) and (H)]. The distribution of hair cells in the Col1A1-pRb$^{-/-}$ utricle was abnormal, as indicated by clustered hair bundles [circles in (F)], in contrast to the normal mosaic pattern in the control (E). In the cochlea, inner hair cells (arrows) and outer hair cells (arrowheads) remained separated by pillar cells, which do not have hair bundles. Uniform orientation of the hair bundles was altered in Col1A1-pRb$^{-/-}$ cochlear hair cells (H). Ut, utricle; Coch, cochlea; IHC, inner hair cell; OHC, outer hair cell. Scale bars, 25 μm.

is not clear whether these supernumerary neurons are highly differentiated or functional.

To identify molecules involved in cell cycle regulation during hair cell development, we studied gene expression in the developing mouse utricle, a balance organ of the inner ear, with the use of oligonucleotide microarrays. We noticed that retinoblastoma family members show a suggestive pattern: From E14.5 to postnatal day (P) 12, *Rb1* expression was constant, *Rbl1* showed down-regulation, and *Rbl2* exhibited up-regulation (*17*). An antibody to pRb weakly labeled all cells in the E12.5 otocyst (fig. S1A), and labeling was prominent in all hair cells from embryo to adult (fig. S1, B to F). Therefore, pRb could be required to suppress cell division in hair cells.

Because germline pRb$^{-/-}$ mice die around E13.5 (*10*), when hair cells are extremely immature, we studied a conditional pRb knockout. Mice with loxP sites flanking exon 19 of the *Rb1* gene (*Rb1*^{loxp}) (*18*) were crossed with mice carrying *cre* under the control of the 3.6-kb collagen 1A1 (Col1A1) promoter, which express *cre* recombinase in a pattern similar to endogenous Col1A1 (*19*). Because these pRb conditional knockout mice (Col1A1-pRb$^{-/-}$) die perinatally, we studied embryos. By in situ hybridization, Col1A1 was detected ubiquitously in the E11.5 otocyst but later reduced in hair cells and supporting cells (fig. S2). In Col1A1-pRb$^{-/-}$ inner ears, pRb was undetectable in the sensory epithelium (Fig. 1, C and D).

If pRb regulates cell cycle exit in hair cells, its loss might permit cell cycle reentry and increase hair cell numbers. We tested this hypothesis by counting cells with hair bundles in E18.5 Col1A1-pRb$^{-/-}$ utricles. Relative to littermate controls, Col1A1-pRb$^{-/-}$ utricles had 40% more cells with bundles [Col1A1-pRb$^{-/-}$: 1406 ± 73 (mean ± SD), $N = 3$; Col1A1-pRb$^{+/-}$: 987 ± 62, $N = 5$; $P < 0.05$] (Fig. 1, E and F). A greater increase in hair bundle number was observed in cochleas. Whereas littermate controls had one row of inner hair cells and three rows of outer hair cells, Col1A1-pRb$^{-/-}$ cochleas had three or four rows of inner hair cells and seven or eight rows of outer hair cells. Most Col1A1-pRb$^{-/-}$ cochlear hair cells had bundles, but many were not properly oriented (Fig. 1, G and H).

The increase in hair cell number in Col1A1-pRb$^{-/-}$ ears suggested that new hair cells arose through an increase in differentiation-competent progenitor cells and/or through continuing hair cell division. To study progenitor cell proliferation, we injected E13.5 pregnant mice with 5-bromo-2′-deoxyuridine (BrdU) 4 hours before embryo harvest. In the primordial organ of Corti, the p27Kip1-positive "zone of nonproliferating cells" (ZPNC) harbors postmitotic sensory precursor cells (*20*). We found BrdU-positive cells in the p27Kip1-positive region of Col1A1-pRb$^{-/-}$ mice (Fig. 2N) but not in controls (Fig. 2M). Therefore, pRb is involved in cell cycle exit of sensory progenitor cells.

To test hair cell proliferation specifically, we injected E16.5 pregnant mothers with BrdU and harvested embryos at E18.5. During normal development, mouse hair cells become postmitotic as early as E12.5 (*21*). As expected, no hair cells or cochlear supporting cells were BrdU-positive in control mice (Fig. 2, I and K). In contrast, many hair cells and cochlear supporting cells were BrdU-positive in Col1A1-pRb$^{-/-}$ mice, indicating that they had entered S phase (Fig. 2, J and L). BrdU labeling in hair cells tended to be weaker than in supporting cells, which suggests that the hair cells had further divided, diluting the BrdU (84% of hair cells were weakly labeled versus 58% of supporting cells, with "weak" considered less than half the level of the brightest supporting cells). We also observed an increased ratio of outer hair cells to Deiters' cells, suggesting contin-

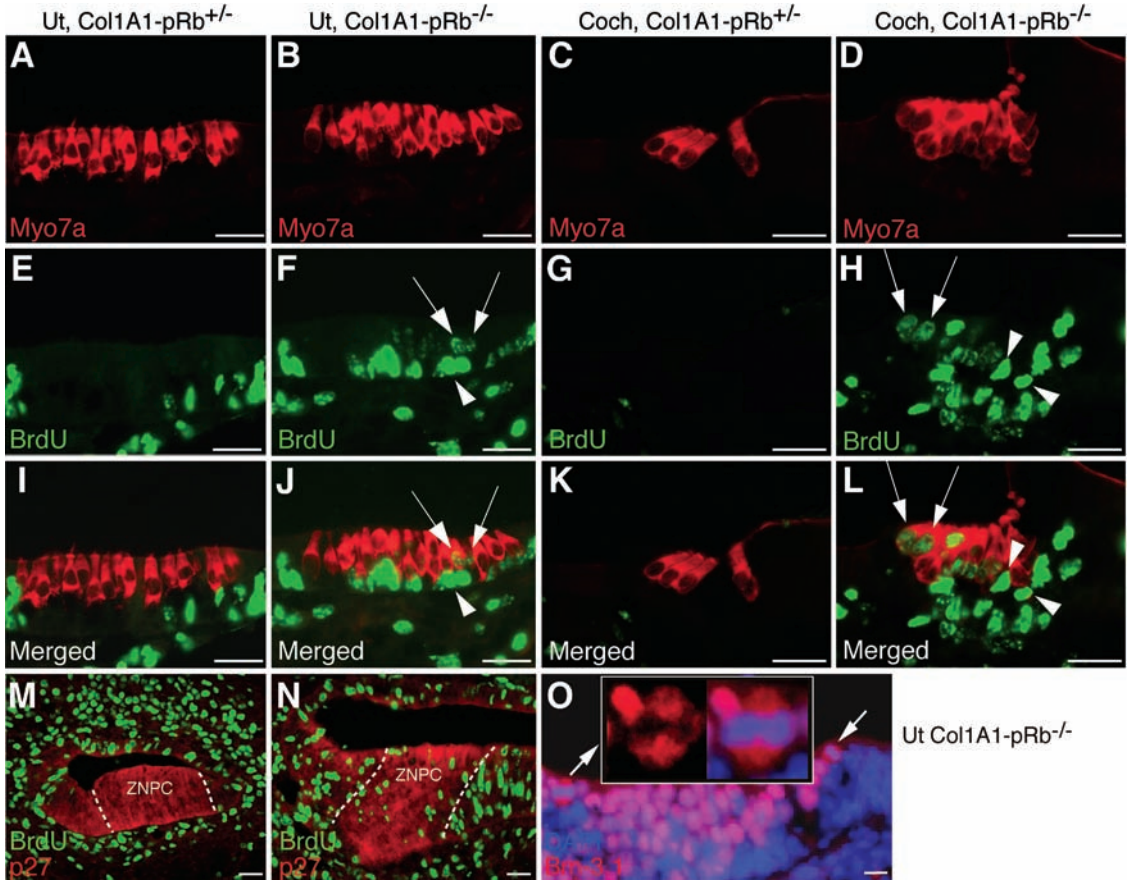

Fig. 2. Sensory progenitor cells and hair cells undergoing mitosis in Col1A1-pRb$^{-/-}$ mice. An antibody to Myo7a labels hair cells. (**A**, **E**, and **I**) In E18.5 control utricular macula, BrdU labeling was not found in hair cells but appeared in some supporting cells. (**B**, **F**, and **J**) In Col1A1-pRb$^{-/-}$ utricular macula, BrdU labeling appeared in both hair cells and supporting cells. (**C**, **G**, and **K**) No BrdU labeling in control cochlear hair cells or supporting cells. (**D**, **H**, and **L**) BrdU labeling of Col1A1-pRb$^{-/-}$ cochlear hair cells and supporting cells. Overall hair cell labeling was weaker (arrows) than supporting cells (arrowheads) [(F), (H), (J), and (L)]. (**M**) No BrdU labeling in control progenitor cells in the ZPNC (demarcated by dashed lines) of the primordial organ of Corti at E13.5. (**N**) BrdU labeling in Col1A1-pRb$^{-/-}$ progenitor cells. (**O**) Hair cells in M phase of cell cycle, as shown by cytoplasmic-like labeling by Brn-3.1 and condensed nuclear labeling by DAPI (arrows). (Inset) A hair cell in M phase with Brn-3.1 alone (left) and Brn-3.1 plus DAPI labeling (right). Scale bars, 25 μm [(A) to (N)], 10 μm (O).

uous hair cell division [Col1A1-pRb$^{-/-}$: ratio = 1.45 ± 0.057 (mean ± SD), N = 51; Col1A1-pRb$^{+/-}$: ratio = 0.79 ± 0.037, N = 22; P < 0.0001]. The proliferation of Col1A1-pRb$^{-/-}$ cochlear supporting cells appeared to be cell specific (fig. S3), as we saw more Deiters' cells than in controls (S100A1 labeling) but not more Pillar cells (p75ntr labeling).

We also identified dividing cells with an antibody to proliferating cell nuclear antigen (PCNA) (*22*). In E13.5 and E18.5 Col1A1-pRb$^{-/-}$ utricles, but not in controls, most hair cells stained strongly for PCNA (fig. S4). In cochleas as well, Col1A1-pRb$^{-/-}$ hair cells and supporting cells were strongly PCNA-positive, unlike controls (fig. S4, M to R). Finally, hair cells in metaphase were observed in E18.5 Col1A1-pRb$^{-/-}$ utricles (Fig. 2O). Staining with 4′,6′-diamidino-2-phenylindole (DAPI) and an antibody to the hair cell–specific transcription factor Brn-3.1 showed that for hair cells in M phase, Brn-3.1 labeling appeared to be cytoplasmic and separated from DAPI-labeled condensed chromosomes that were segregating into two daughter nuclei during mitosis (Fig. 2O, arrows and inset).

Most apical hair cells in E18.5 Col1A1-pRb$^{-/-}$ utricles showed highly differentiated morphology, including pear-shaped cell bodies and intact hair bundles. Hair bundles were labeled with antibodies to espin (an actin cross-linker) and Ptprq (present in highly differentiated cochlear hair bundles) (Fig. 3, A to D) (*23*, *24*). An antibody to tubulin revealed, as in controls, nerve fibers surrounding most Col1A1-pRb$^{-/-}$ hair cells (Fig. 3, E and F), and an antibody to the synaptic vesicle protein synaptophysin showed labeling around many Col1A1-pRb$^{-/-}$ hair cells (fig. S5), suggesting that Col1A1-pRb$^{-/-}$ hair cells can attract axons and form synapses. Other markers of differentiated hair cells were also detected in Col1A1-pRb$^{-/-}$ mice, including Brn-3.1 (Fig. 2O), Lhx3 (Fig. 3, B and D), Gfi1, Math1, calretinin, and parvalbumin 3. In contrast to a conditional pRb$^{-/-}$ mouse model where retinal rods failed to differentiate (*25*), cell fate determination and subsequent differentiation were largely intact in the proliferating Col1A1-pRb$^{-/-}$ hair cells. Therefore, Col1A1-pRb$^{-/-}$ hair cells become differentiated without switching off proliferation, indicating that hair cell fate determination and differentiation do not require pRb function.

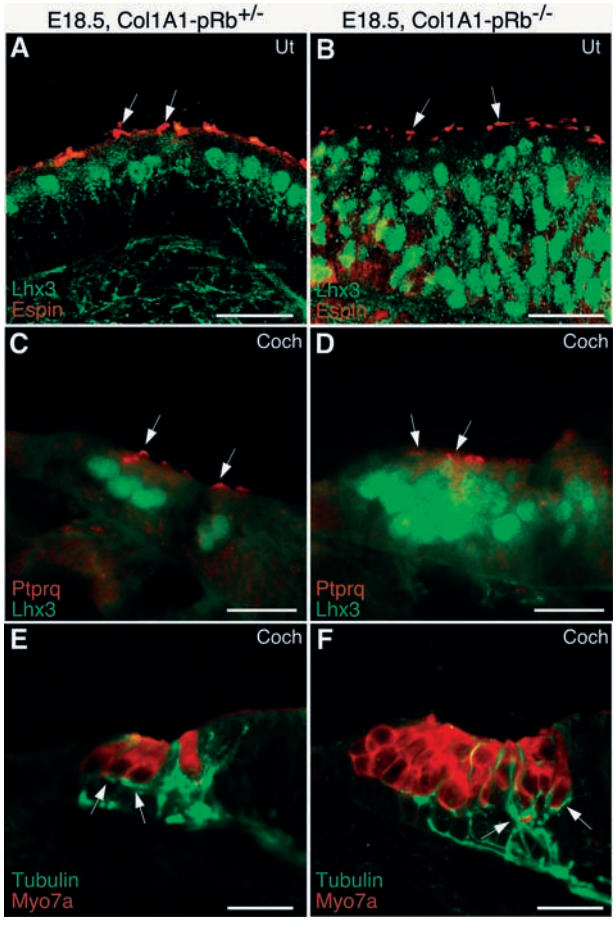

Fig. 3. Hair cells labeled with differentiating hair cell markers. (**A** to **D**) Lhx3 labels hair cell nuclei. Antibodies to espin labeled hair bundles (arrows) in control (A) and Col1A1-pRb$^{-/-}$ utricles (B). Antibodies to Ptprq labeled hair bundles (arrows) in control (C) and Col1A1-pRb$^{-/-}$ cochleas (D). (**E** and **F**) Antibodies to tubulin labeled nerve fibers surrounding hair cells marked with Myo7a (arrows) in control (E) and Col1A1-pRb$^{-/-}$ cochleas (F). Note labeling surrounding multiple inner hair cells in the Col1A1-pRb$^{-/-}$ cochlea (F). Scale bars, 25 μm.

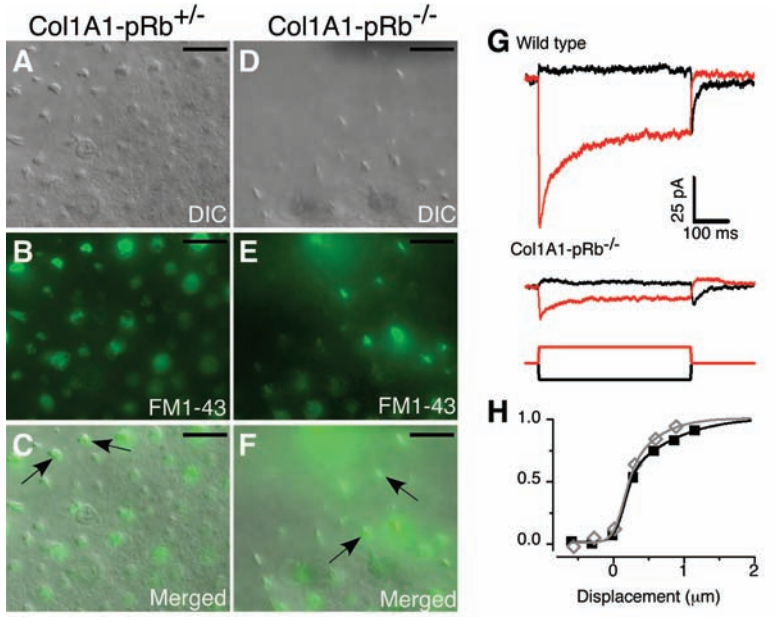

Fig. 4. Functional mechanotransduction by Col1A1-pRb$^{-/-}$ and control hair cells at E18.5. (**A** to **F**) FM1-43 accumulation by utricular hair cells. After exposure to FM1-43 for 1 min, most hair bundles [differential interference contrast images, (A) and (D)] were labeled with FM1-43 [green, (B) and (E)] in both control [(A) to (C)] and Col1A1-pRb$^{-/-}$ [(D) to (F)] mice, indicating that these cells had functional mechanotransduction channels. Arrows indicate clearly labeled bundles. (**G**) Transduction currents elicited in control (top) and Col1A1-pRb$^{-/-}$ (middle) littermates by step deflections of the hair bundle (bottom). Adaptations of the transduction currents in response to positive (red) and negative (black) hair bundle deflections were revealed. The wild-type response is typical of transduction currents in neonatal mice (*31*). However, transduction currents in Col1A1-pRb$^{-/-}$ mice were small: Peak transducer current (mean ± SEM) was 14.2 ± 2.9 pA (n = 4). (**H**) Normalized current-displacement relations for the control and Col1A1-pRb$^{-/-}$ transduction currents shown in (G). These two hair cells had similar operating ranges. Scale bars, 10 μm.

The sine qua non of hair cell function is mechanosensitivity. FM1-43, a fluorescent dye, enters hair cells through open mechanotransduction channels and so serves as a vital optical assay for mechanosensitivity (*26*, *27*). We observed FM1-43 labeling in bundles and cell bodies of most hair cells in both control (Fig. 4, A to C) and Col1A1-pRb$^{-/-}$ utricles (Fig. 4, D to F). Because most hair cells in Col1A1-pRb$^{-/-}$ utricles are PCNA-positive, FM1-43 entry can occur in cycling hair cells.

We then recorded transduction currents in control and Col1A1-pRb$^{-/-}$ hair cells. Transduction currents were evoked in four randomly selected Col1A1-pRb$^{-/-}$ hair cells (Fig. 4, G and H), although currents were smaller than in controls (10 to 20 pA versus ~200 pA in controls). Currents might be smaller if bundles had little time to develop between cell divisions, especially with the known delay between bundle formation and transduction (*28*). Transduction currents showed a normal activation range and adaptation time course. Thus, specialized hair cell function does not require pRb.

To determine whether apoptosis occurs in Col1A1-pRb$^{-/-}$ hair cells, we assayed for activated caspase-3. We did not detect any caspase-3–positive cells in Col1A1-pRb$^{-/-}$ sensory epithelium nor in controls (fig. S6). Therefore, loss of pRb itself does not appear to lead to cell death in the inner ear.

The prominent expression of *Rb1* in postnatal hair cells and the fact that acute loss of pRb causes cell cycle reentry in quiescent or senescent cells (*29*) suggests a role for pRb in maintaining hair cells' nonproliferative status. To test this hypothesis, we cultured floxP-pRb utricles and infected them with adenovirus carrying *cre* recombinase, acutely deleting the *Rb1* gene in infected hair cells (*30*). Utricular hair cells are mature at P10 and postmitotic at both stages studied (E17.5 and P10). After continuous culture in the presence of BrdU, no labeling was detected in hair cells infected with adenovirus carrying green fluorescent protein (GFP) (Fig. 5, A to D) or in uninfected floxP-pRb hair cells (Fig. 5, F and H, arrows), whereas hair cells infected with adenovirus carrying *cre* recombinase incorporated BrdU (Fig. 5, E to H). There were fewer BrdU-labeled hair cells in P10 cultures than in E17.5 cultures, likely because of the lower efficiency of infection of P10 hair cells. Additionally, more pRb was present in infected P10 hair cells after culture, which suggests that *cre*-mediated recombination or pRb degradation was less efficient in P10 cultures. All the infected hair cells lost hair bundles (*30*), so we could not test function. Nonetheless, the damaged hair cells reentered the cell cycle.

Cochleas in Col1A1-pRb$^{-/-}$ mice were studied for conversion of supporting cells to hair cells. If this were the main pathway for increased hair cell number, we would expect that p27Kip1-labeled supporting cells would label with Math1 (the earliest hair cell marker) or that Math1-positive cells would appear in supporting cell regions outside the hair cell region. However, in neither case did we find such cells. Although we cannot completely exclude cell fate conversion, it is most likely that increased hair cell precursors and subsequent hair cell division are primarily responsible for the overproduction of hair cells.

We have shown that differentiated mammalian hair cells can continue to cycle and divide in the absence of pRb, so that functional hair cells can be generated through divisions of preexisting hair cells. Furthermore, acute ablation of pRb in differentiated hair cells led to cell cycle reentry. The demonstration that pRb critically regulates hair cell division opens new opportunities for hair cell regeneration and for creating cell lines for hearing research. For hair cell regeneration, it will be important to determine whether a reversible block of pRb function in hair cells might be achieved in place of permanent deletion of the *Rb1* gene. Thus, the regulated inactivation of pRb—through the use of small interfering RNA (siRNA), a small-molecule inhibitor of pRb, or reversible manipulation of pRb-modifying kinases—may result in production of functional hair cells followed by restoration of normal cell cycle exit. These results also show that an irreversible switch from proliferation is not required for "terminal" differentiation, because cycling cells in the absence of pRb are highly differentiated and functional. Our findings may have implications for regenerating other functional cells through manipulation of negative cell growth control genes.

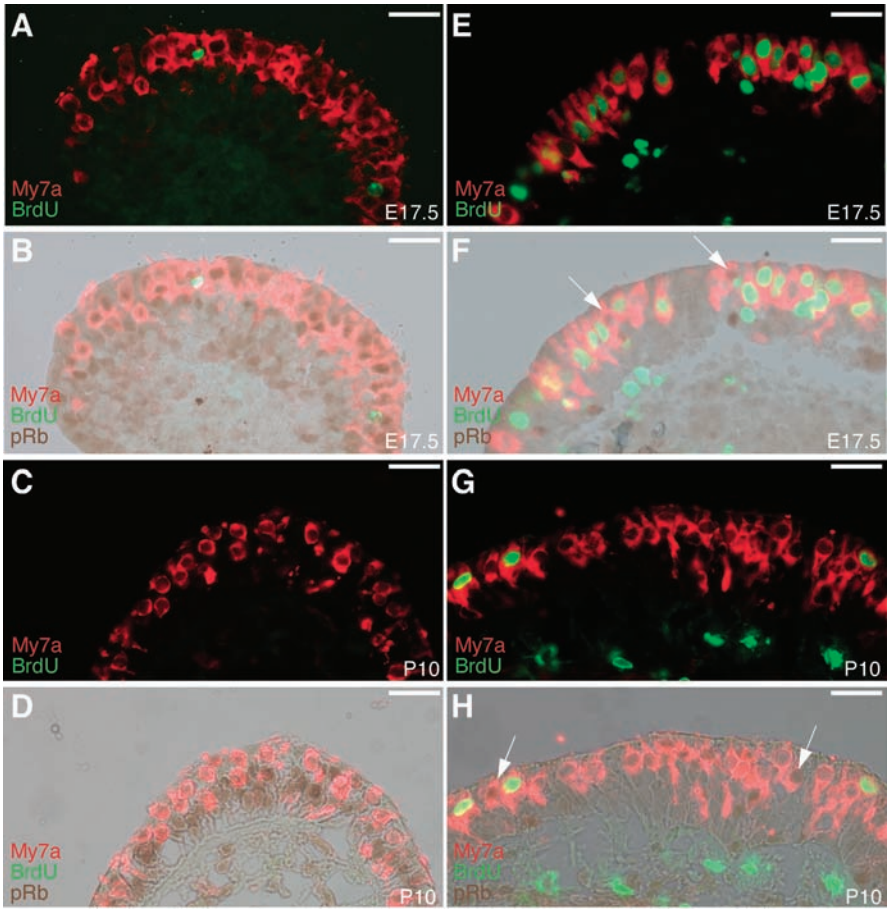

Fig. 5. Cell cycle reentry by postmitotic hair cells after acute deletion of the *Rb1* gene. (**A** to **D**) floxP-pRb utricles at E17.5 [(A) and (B)] and P10 [(C) and (D)] were infected with adenovirus carrying GFP as controls, then cultured with addition of BrdU. All hair cells are pRb-positive and BrdU-negative. The two BrdU-positive cells [(A) and (B)] are not hair cells. (**E** to **H**) floxP-pRb utricles at E17.5 [(E) and (F)] and P10 [(G) and (H)] were infected with adenovirus carrying *cre* recombinase and GFP. Cell cycle reentry by the infected hair cells (pRb-negative) was shown by BrdU labeling [(F) and (H)]. As an internal control, no BrdU labeling was in the uninfected hair cells (pRb-positive, arrows). Scale bars, 25 μm.

References and Notes

1. J. T. Corwin, D. A. Cotanche, *Science* **240**, 1772 (1988).
2. B. M. Ryals, E. W. Rubel, *Science* **240**, 1774 (1988).
3. A. Forge, L. Li, J. T. Corwin, G. Nevill, *Science* **259**, 1616 (1993).
4. M. E. Warchol, P. R. Lambert, B. J. Goldstein, A. Forge, J. T. Corwin, *Science* **259**, 1619 (1993).
5. H. Lowenheim *et al.*, *Proc. Natl. Acad. Sci. U.S.A.* **96**, 4084 (1999).

6. P. Chen *et al.*, *Nature Cell Biol.* **5**, 422 (2003).
7. M. Classon, E. Harlow, *Nature Rev. Cancer* **2**, 910 (2002).
8. M. M. Lipinski, T. Jacks, *Oncogene* **18**, 7873 (1999).
9. M. Classon, N. Dyson, *Exp. Cell Res.* **264**, 135 (2001).
10. T. Jacks *et al.*, *Nature* **359**, 295 (1992).
11. K. L. Ferguson, R. S. Slack, *Neuroreport* **12**, A55 (2001).
12. D. M. Thomas *et al.*, *Mol. Cell* **8**, 303 (2001).
13. R. S. Slack, H. El-Bizri, J. Wong, D. J. Belliveau, F. D. Miller, *J. Cell Biol.* **140**, 1497 (1998).
14. K. L. Ferguson *et al.*, *EMBO J.* **21**, 3337 (2002).
15. D. MacPherson *et al.*, *Mol. Cell. Biol.* **23**, 1044 (2003).
16. S. Marino, D. Hoogervoorst, S. Brandner, A. Berns, *Development* **130**, 3359 (2003).
17. Z.-Y. Chen, data not shown.
18. M. Vooijs, H. te Riele, M. van der Valk, A. Berns, *Oncogene* **21**, 4635 (2002).
19. F. Liu *et al.*, *Int. J. Dev. Biol.* **48**, 645 (2004).
20. P. Chen, J. E. Johnson, H. Y. Zoghbi, N. Segil, *Development* **129**, 2495 (2002).
21. M. Xiang, W. Q. Gao, T. Hasson, J. J. Shin, *Development* **125**, 3935 (1998).
22. A. L. Woods *et al.*, *Histopathology* **19**, 21 (1991).
23. L. Zheng *et al.*, *Cell* **102**, 377 (2000).
24. R. J. Goodyear *et al.*, *J. Neurosci.* **23**, 9208 (2003).
25. J. Zhang *et al.*, *Nature Genet.* **36**, 351 (2004).
26. J. E. Gale, W. Marcotti, H. J. Kennedy, C. J. Kros, G. P. Richardson, *J. Neurosci.* **21**, 7013 (2001).
27. J. R. Meyers *et al.*, *J. Neurosci.* **23**, 4054 (2003).
28. G. S. Geleoc, J. R. Holt, *Nature Neurosci.* **6**, 1019 (2003).
29. J. Sage *et al.*, *Nature* **424**, 223 (2003).
30. J. R. Holt *et al.*, *J. Neurophysiol.* **81**, 1881 (1999).
31. M. A. Vollrath, R. A. Eatock, *J. Neurophysiol.* **90**, 2676 (2003).

32. We thank L. Goodrich, D. Fekete, M. Holley, and J. Macklis for critical comments on the manuscript. D.P.C. is an Investigator of the Howard Hughes Medical Institute. Supported by NIH grants DC-04546 (Z.-Y.C.), DC-00200 (J.T.C.), and DC-AG20208 (P.W.H.) and by a Pfizer/AFAR Innovations in Aging Research grant (Z.Y.C.).

Supporting Online Material
www.sciencemag.org/cgi/content/full/1106642/DC1
Materials and Methods
Figs. S1 to S6
References

22 October 2004; accepted 3 January 2005
Published online 13 January 2005;
10.1126/science.1106642
Include this information when citing this paper.

Learned Predictions of Error Likelihood in the Anterior Cingulate Cortex

Joshua W. Brown* and Todd S. Braver

The anterior cingulate cortex (ACC) and the related medial wall play a critical role in recruiting cognitive control. Although ACC exhibits selective error and conflict responses, it has been unclear how these develop and become context-specific. With use of a modified stop-signal task, we show from integrated computational neural modeling and neuroimaging studies that ACC learns to predict error likelihood in a given context, even for trials in which there is no error or response conflict. These results support a more general error-likelihood theory of ACC function based on reinforcement learning, of which conflict and error detection are special cases.

Despite remarkable recent advances in cognitive neuroscience, it remains unclear how the brain learns to exert cognitive control over behavior. ACC and neighboring areas in the frontal medial wall play a role in monitoring and controlling goal-directed behavior (*1*–*3*). Error-related negativity (ERN/Ne) (*4*–*6*) and single-unit studies propose that ACC detects errors as discrepancies between actual and intended events (*7*). Alternatively, ACC may detect conflict between mutually incompatible response processes (*8*–*10*) such as incorrect versus correct responses. However, it has not been clear how the ACC learns what constitutes an error or that a given set of responses conflict. We develop here a computational model that demonstrates how ACC might not detect conflict or errors per se but rather more generally represent a prediction of error likelihood (*11*). In particular, the model makes a very specific prediction regarding ACC activity dynamics: The ACC response to a given task condition will be proportional to the perceived likelihood of an error in that condition.

The error-likelihood hypothesis also posits a training signal by which stimulus-specific ACC effects are acquired. This training signal may be dopaminergic. Phasic midbrain dopamine neuron activity is critically involved in reinforcement learning (*12*, *13*), and phasic suppression of dopamine apparently drives the ERN/Ne (*11*). Thus, phasic dopamine suppression occurring in response to errors might serve as a training signal (*14*, *15*) that causes ACC to respond more strongly to contexts in which errors are more frequent.

We formalized the error-likelihood hypothesis as a computational neural model to (i) examine how ACC representations might develop through experience and (ii) explicitly investigate the implications of the hypothesis (*16*). To test the model, we used a change variant (Fig. 1) of the well-known stop-signal paradigm used to examine inhibitory control (*17*). Previous work has demonstrated that stop-signal trials are associated with increased ACC activity in humans (*18*) and related medial frontal areas in other primates (*7*, *19*). The task consisted of conditions associated with high and low error rates crossed with the presence or absence of response conflict. Comparison of correct trials without response conflict across high and low error-rate conditions afforded assessment of error-likelihood effects while controlling for response conflict and errors.

In the computational model (Fig. 2A), simulated ACC neuron units received inputs repre-

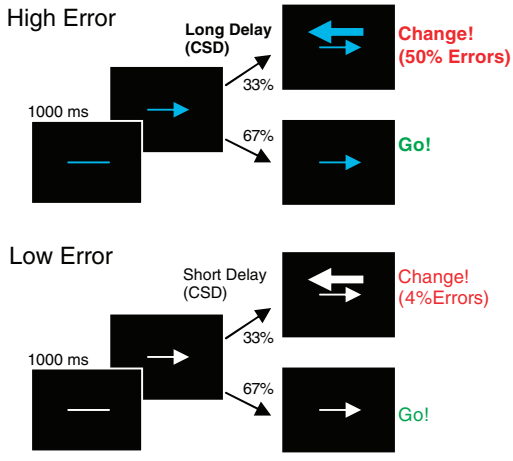

Fig. 1. Change signal task. An initial difficulty cue (plain line) appeared for 1000 ms. For a given trial, cue color (white or blue, equiprobable and randomly intermixed) predicts low versus high error likelihood, respectively. Then a go signal was presented (left- or right-pointing arrow made by extending the plain line to → or ←) that indicated the required button-press response (left index finger for left arrow and right index finger for right arrow). On 33% of the trials, a change (conflict) signal was added to the go signal after a variable CSD relative to go signal onset. This change signal (a second, larger arrow appearing above the first and pointing in the opposite direction) indicated that the response had to be left-right reversed from that indicated by the go signal. Both change and go signals remained visible until a response deadline of 1000 ms after go signal onset. A 500-ms blank interval occurred before the onset of the next trial. All stimuli for a given trial were the same color. Error rates were explicitly set and controlled by dynamically adjusting the CSDs for each error-likelihood condition independently with the use of a staircase algorithm. The low-error condition had shorter CSDs, whereas the high-error condition had longer CSDs, reflecting the well-established positive monotonic relationship between CSD and error rate in stop-signal tasks (*17*).

Department of Psychology, CB 1125, Washington University, St. Louis, MO 63130, USA.

*To whom correspondence should be addressed. E-mail: jwbrown@artsci.wustl.edu